Inserting Buffer Layers for Carrier Balance Configurations in Hyperfluorescence-Based OLEDs

Nobuto Managaki, Mizuki Oka, Masashi Tsubuku, Hiroyuki Kimura
Japan Display Inc., Chiba, Japan

Abstract
OLEDs, containing non-doped emissive layers as buffer layers, restored their device characteristics of red, green hyperfluorescence, and blue triplet–triplet fusion. These features degraded owing to carriers accumulated at the heterostructures. We considered the built-in voltage and nonradiative recombination processes as the effects of disturbing carrier balance.

Author Keywords
OLED; hyperfluorescence; TADF; carrier balance; surface accumulation; buffer layer

1. Introduction
The development of hyperfluorescence (HF) device structures has become the subject of recent progress, focusing on highly efficient, cost-efficient, and pure-color organic light-emitting diodes (OLEDs). These devices incorporate thermally activated delayed fluorescence (TADF) materials and, fluorescence dopants (FDs). The HF layer components offer functions not present in phosphorescent materials, with fluorescent dopants defining the color gamut as the final emitter, thereby enabling vivid displays [1-2]. The TADF molecular designs and the adjustment of energy transfer parameters significantly affect OLED efficiency. However, improper alignment of the multistacked layers can degrade device features, like driving voltage, efficiency, and device lifetime (LT95) [3-4]. Emissive layer systems with highly doped FDs or TADF materials cause a mix of a few nonradiative recombination processes via exciplex, polaron, and energy transfer from bulk-like TADF materials. Moreover, charge accumulation at heterostructures leads to large electrical and optical losses in OLEDs, predicted by capacitance-voltage (CV) curves [5].

In OLED markets, cost-saving becomes crucial, on the one hand by using emissive layers (EMLs) without noble metals, on the other hand by reducing the number of evaporation-process masks. To reduce fine metal masks during OLED evaporation, the OLED displays should have common layers between red, green, and blue OLEDs, like the hole injection layer (HIL) and the hole transport layer (HTL). This study proposes a cost-efficient organic heterostructure comprising red and green HF-OLEDs and blue fluorescent OLEDs (F-OLEDs), as indicated in Figure 1. These OLEDs are compatible with less fine mask usage procedure on the bright side, owing to numerous common layers described in latter sections. However, the required carrier balances differ for each color, affecting device features in terms of electrical recession. Therefore, we examined the effect of buffer layers, inserting them between the EML and the blocking layer, to mitigate losses. First, the carrier balance of green HF-OLEDs was mostly optimized, arranging the electron blocking layer (EBL) materials as a common layer. Next, buffer layers were formed at the surface between the red-EML and the common EBL, compared with the HF-OLED that did not contain any buffer layer. We also verified the effectiveness of other buffer layers at the surface of the blue EML and the common hole blocking layer (HBL) in the F-OLED. This approach resulted in achieving a wide color gamut with efficiency competitive with phosphorescent OLED (Ph-OLED) products.

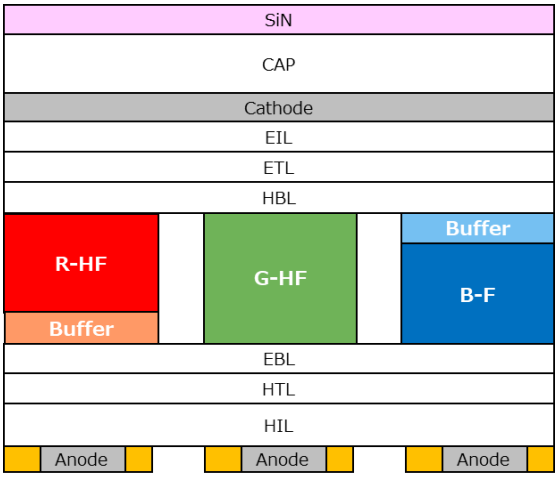

Figure 1. Schematic of HF-based OLEDs containing G-HF, R-HF, and B-F devices.

2. Experiment and OLED structures
A schematic image of the cost-efficient HF-based OLED is shown in Figure 1. Initially, common layers, including the HIL, HTL, and EBL were deposited on an indium tin oxide. Next, red-HF, green-HF, and blue-F EMLs with buffer layers were formed using fine evaporation masks for each color, applied on the common layers. Following this, additional common layers such as the HBL, electron transport layer, and electron injection layer were formed beneath a MgAg semitransparent cathode. Finally, an insulating layer and SiN encapsulation were applied to fabricate the microcavity structures. We measured the electrical properties of the OLEDs such as JV curves, normalized external quantum efficiency (EQE), LT95, and CV curves using impedance spectroscopy. The temperature and the current density during the LT95s measurement were 308 K and 50 mA/cm^2.

3. Results and Discussions

Table 1. List of green HF-OLEDs with various EBL materials

	Voltage	Efficiency	LT95
HF_BE	V	cd/A	h
EBL-1 ΔE_{LUMO} **= 0.2 eV**	4.10	65.4	23
EBL-2 ΔE_{LUMO} **= 0.0 eV**	3.91	73.7	39
EBL-3 ΔE_{LUMO} **= 0.1 eV**	3.86	81.6	44

ISSN 0097-996X/25/5603-2224-$1.00 © 2025

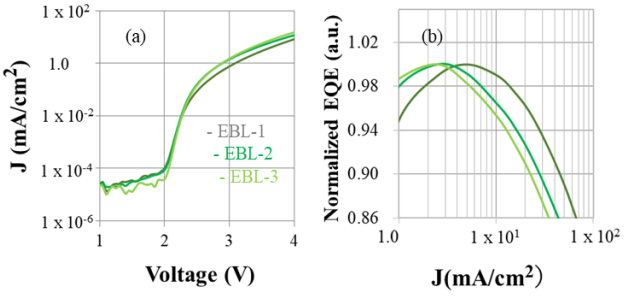

Figure 2. (a) JV curves of the green HF-OLEDs and (b) normalized EQEs.

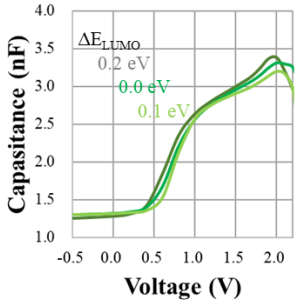

Figure 3. CV curves of the green HF-OLEDs.

3.1 ΔE_{LUMO} between EBL and EML in Green HF-OLED: In a previous letter [5], bottom emission (BE) green HF-OLEDs were discussed, where we modified carrier densities, TADF materials, and the material ratios in the blended EMLs. These parameters influenced significantly, the carrier balance in the EMLs. In this study, three EBL materials were chosen to examine the impacts of ΔE_{LUMO} between the EBLs and the EML on carrier flow. Table 1 presents the characteristics of HF-OLEDs. The ΔE_{LUMO} at the surface of EBL-1, -2, and -3 are, 0.2, 0.0, 0.1 eV, respectively, showing improvement in device performance in this turn. Figures 2 (a) and (b) illustrate JV curves and normalized EQEs. The JV curves shifted toward higher voltages at around 1.0 mA/cm^2, and EQEs degraded at current densities below1.0 mA/cm^2, when using inappropriate EBLs. Figure 3 presents the CV curves of the green HF-OLEDs, demonstrating carrier accumulation in the green EML, which depend on the EBL materials. In the graph, larger lowest unoccupied molecular orbital levels between the EBL and EML caused carrier accumulation at the surface, while too small energy barriers at the surface also caused another carrier accumulation by allowing easy electron path into HTL. These paths result in electron-hole compensation and a depletion of hole in the HTL, leaving a large number of electrons unused in the EML. such conditions affected the JV features, and efficiencies, indicating increased resistance between EBL and EML arising from built-in voltage [6], and decreased efficiency owing to recombination processes, like exciplex or polaron formations, which are attribute to large number of electrons, trapped in the EML. The implications and CV curves illustrate the device features well. The capacitances between 0.5 and 1.5 V show the carrier-injection into green EML layers. At around 2.0 V, these values mainly indicate radiative recombination processes via the HF system, which also includes nonradiative recombination processes. In the CV curves, inappropriate EBLs caused a bult-in voltage and nonradiative recombination in the EML. Thus, we can conclude that the EBL-3 is likely the most optimized layer.

Table 2. List of red HF-OLEDs with various buffer layer thicknesses.

	Voltage	Efficiency	EQE
HF_BE	V	cd/A	%
EBL-4	3.92	26.3	13.7
EBL-3	4.40	20.7	10.2
EBL-3 with 5 nm-Buffer	4.24	27.6	13.6
EBL-3 with 6.3 nm-Buffer	4.13	26.3	13.9
EBL-3 with 7.5 nm-Buffer	4.07	27.2	15.0

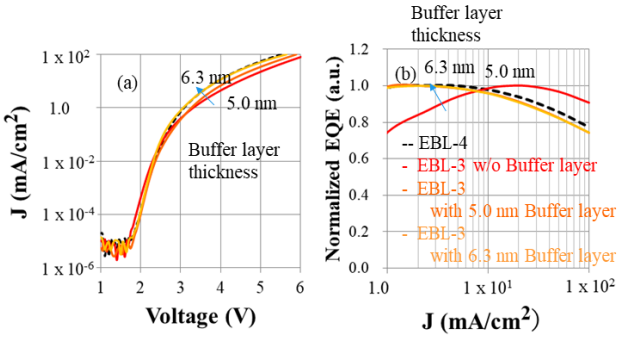

Figure 4. JV curves of the red HF-OLEDs (a) and normalized EQE (b).

3.2 Effects of Buffer Layers between Red-EML and EBL: In this section, we compared two EBLs in red HF-OLEDs: EBL-3 and EBL-4. As shown in the previous section, EBL-3 was used for green HF-OLEDs, and our challenge is to achieve efficient red HF-OLEDs with EBL-3 as a common layer between red and green devices. BE red HF-OLEDs were fabricated, using EBL-3 with buffer layers and EBL-4 without any buffer layers. Table 2 presents the HF-OLED features. ΔE_{LUMO} between the red-EML and EBL-3 and, that of EBL-4 are 0.15 eV, and 0.1 eV, respectively. In the red HF-OLEDs, we inserted non-doped EMLs as buffer layers, between EBL-3 and the red-EML, modifying their thicknesses, to alleviate the effects of carriers accumulated at the surface. Figure 4 (a) and (b) show the JV curves and normalized EQEs. The JV curves shifted toward higher voltage at current densities in the saturated region, and the EQEs significantly degraded at lower current density sides, when using EBL-3 (a common EBL), compared with EBL-4 (a mostly optimized EBL). Similarly to green HF, we consider that large electrical barrier caused the carrier accumulation at the surface, leading to an increase in device resistance, and a large degradation in the device efficiencies. However, the JV curves and efficiencies of the OLEDs with buffer layers returned to those of the red HF-

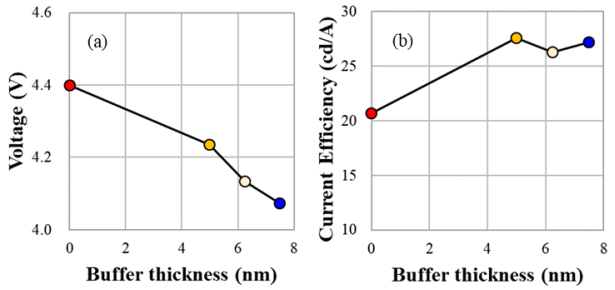

Figure 5. Voltages (c), and efficiencies of the red HF-OLEDs, plotted at a current density of 10 mA/cm^2 (d).

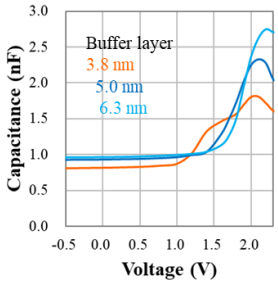

Figure 6. CV curves of the red HF-OLEDs.

OLEDs with EBL-4. This indicates that inserting buffer layers restored device features mostly. As shown in Figures 5 (a) and (b), we plotted the driving voltages and efficiencies at 10 mA/cm^2 as a function of buffer thickness. The driving voltages improved, and efficiencies restored their features with increased the buffer layer thickness. Figure 6 shows the CV curves of the red HF-OLEDs as a function of buffer layer thickness. In the graph, the capacitances between 1.0 and 1.5 V indicate carrier injection into the red EMLs. At around 2.0 V, the region encompasses both radiative and nonradiative recombination, but their carriers in the region mainly indicate nonradiative processes, like triplet-triplet annihilation (TTA) in addition to the nonradiative processes described above. In the graph, capacitances quench at around 1.5 V, while they increase at around 2.0 V as the buffer layer thickness increased. These results also illustrate the red HF-OLEDs with buffer layer well. The buffer layers gave us smooth carrier injection into the red EML, preventing the consumption of electron–hole pairs through nonradiative recombination paths. We consider the effects of buffer layer on the HF-OLEDs as electron diffusion in the non-doped EML, allowing the prevailing charges to mitigate the degradations in the HF features: built-in voltage, regarding driving voltage, and nonradiative recombination, such as exciplex, polaron, and TTA. Thus, this effectively enhances the performance of HF-OLEDs with the buffer layer.

3.3 Effects of Buffer Layers between Blue-EML and HBL: We verified the top emission (TE) blue F-OLEDs with buffer layers, deposited under the HBL, arranging thicknesses of the buffer layer, to achieve well-aligned carrier balances in the EML. As demonstrated in the experiments, the same HBL material was used as a common layer for the red, green HF-OLEDs, and blue F-OLEDs. Table 3 presents the features of the F-OLEDs. Figures 7 (a) and (b) show the JV curves and normalized EQEs. The JV curves shifted toward lower voltages at

Table. 3 List of blue F-OLEDs with various buffer layer thicknesses.

	Voltage	Efficiency	EQE	FWHM	CIEx	
Top Emission	V	cd/A	%	nm	x	y
HBL	4.19	4.80	12.3	15.5	0.145	0.034
HBL with 1.0 nm-Buffer	4.45	5.94	12.9	19.7	0.141	0.043
HBL with 2.0 nm-Buffer	4.34	5.98	13.2	19.6	0.140	0.043
HBL with 3.0 nm-Buffer	4.21	5.97	13.1	19.4	0.141	0.042
HBL with 4.0 nm-Buffer	4.07	6.36	14.5	19.0	0.142	0.040
HBL with 5.0 nm-Buffer	3.77	6.99	15.8	17.2	0.142	0.040

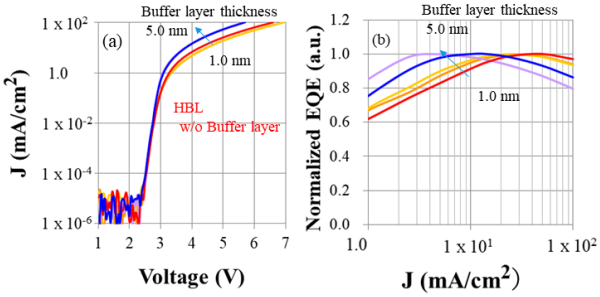

Figure 7. JV curves of the blue F-OLEDs (a) and, normalized EQE (b).

current densities in saturated region, and the EQEs were enhanced at smaller current density sides, as the thickness of the buffer layer increased. In Figures 8 (a) and (b), we plotted the driving voltages and efficiencies at 10 mA/cm^2 as a function of buffer thickness. Similarly to the red HF-OLEDs, the blue F-OLED performance improved with increased buffer thickness. Figure 9 displays the CV curves. Capacitances decreased as the buffer thickness increased. Moreover, each curve was broad with some exhibiting two peaks. The lower voltage peaks represent carriers used for singlet emissions, whereas the higher voltage peaks relate to carriers injected into the triplet state for triplet-triplet fusion (TTF), indicating radiative recombination processes. Thus, decreased capacitance is attributed to smooth carrier injections into the radiative sites in the EMLs. Moreover, changes in capacitance indicate a relaxation of charges between the bule EMLs and the HBL. We also consider the buffer layer's effect on F-OLEDs as facilitating electron accumulation. However, to avoid excess charge, the thickness of the buffer layer should be carefully arranged. These results suggest that buffer thickness affects driving voltages and efficiencies in the F-OLEDs. As shown in sections 3.2 and 3.3, carrier balance configurations are available through buffer layers in both HF-OLEDs and F-OLEDs.

3.4 TE Features of TEGs using Red, Green HF-OLEDs and Blue F-OLED with Buffer Layers: The HF-based OLEDs with buffer layers are compared to our latest Ph-based OLED products. Table 4 summarizes the electrical properties of these OLEDs in the test element groups (TEGs). Figure 10 illustrates the chromaticity from these OLEDs. In our products, green and red OLEDs utilized phosphorescent EMLs, while the blue OLED was fluorescent. Conversely, in HF-based OLEDs, green and red EMLs contained fluorescent dopants and TADF materials; in addition, the red-HF and the blue-F had

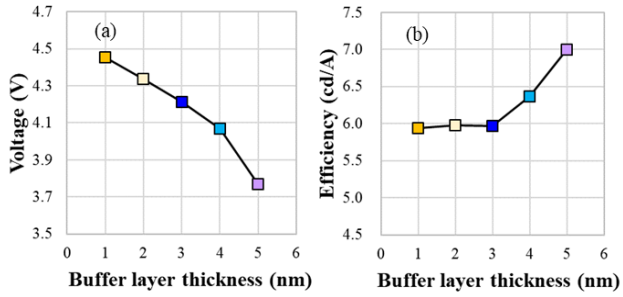

Figure 8. Voltages (a), and efficiencies of the blue F-OLEDs, plotted at a current density of 10 mA/cm^2 (b).

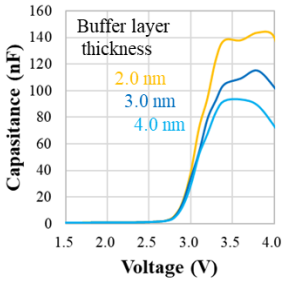

Figure 9. CV curves of the blue F-OLEDs.

buffer layers in each heterostructure. All EMLs were formed between common layers, using the procedures described in the section 2. In the green HF-OLED, the driving voltage was comparable, but the efficiency was significantly higher than green Ph-OLED. The red HF-OLED with a buffer layer had a driving voltage and efficiency mostly identical to those of Ph-OLED but offered greater durability despite the red-EML being deposited on the common EBL. Furthermore, the blue F-OLED with a buffer layer demonstrates device features were also mostly same as these of the F-OLED product with appropriate HBL, when the blue EML was deposited beneath the common HBL for HF-OLEDs. We achieved efficient OLEDs containing green, and red hyperfluorescence, and blue fluorescence by forming buffer layers between EMLs and blocking layers. Furthermore, the HF-based OLEDs covered 99.9% of the DCP-I3.

4. Conclusion

As evidenced in previous sessions, OLEDs with buffer layers revealed various effects on the JV curve, efficiency, and LT95. This insight allows us to maximize the use of common layers without experiencing electrical recessions. Initially, we found an EBL as a common layer for HF-based displays, primarily by optimizing the layer materials in green HF- OLEDs.

Table 4. List of Ph- and HF-based OLEDs.

	Voltage	Efficiency	FWHM	CIE		LT95
Top Emission	V	cd/A	nm	x	y	h
G-Ph	3.88	142	18.1	0.189	0.760	43
R-Ph	4.23	74.5	18.7	0.681	0.318	80
B-FL	3.66	7.12	16.9	0.145	0.036	80
G-HF	3.89	191	17.3	0.192	0.767	29
R-HF with Buffer	4.35	73.8	17.0	0.683	0.317	420
B-FL with Buffer	3.77	6.99	17.2	0.142	0.040	91

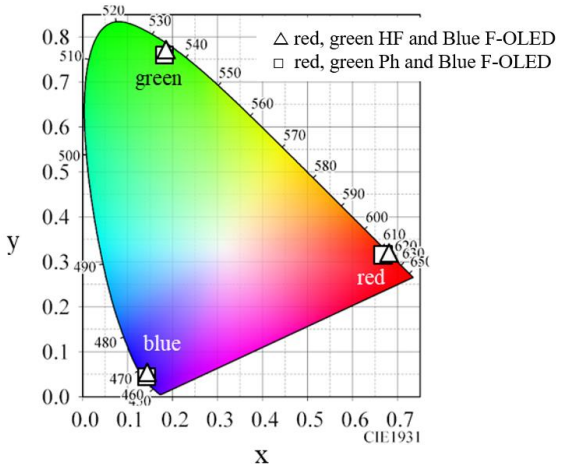

Figure 10. Chromaticity of the EL from the Ph- and HF-based OLEDs.

Subsequently, non-doped EML was implemented as a buffer layer between the red EML and the common EBL. Furthermore, another buffer layer was introduced between the blue EML and a common HBL, restoring the device properties of the red and blue OLEDs. We believe that the extent of carrier accumulation is key to understanding the recessions, affecting built-in voltage and recombination processes, such as TTA and TTF. These results highlight the significant impact of buffer layers in improving device performance.

5. Acknowledgements

The authors would like to thank the members of Kyulux, Inc. for providing various TADF-related materials.

6. References

[1] Junji A, Shuo-Hsien C, Hayao K, Ayataka E. Highly efficient and narrowband emission for BT. 2020. Proc. IDW. 2023;31:558-561.

[2] Fan XC, Wang K, Shi YZ, Cheng YC, Lee YT, Yu J. Ultrapure green organic light-emitting diodes based on highly distorted fused π-conjugated molecular design. Nature Photonics. 2023;17(3):280-285.

[3] Hayer A, Eickhoff C, Ganss S, May F, Montenegro E, Kraska M, Kroeber J, Parham A, Stolz S. Tailored hosts for shaping the emissive layer of green phosphorescent OLEDs. Proc. IDW. 2023;30:1-10.

[4] Yutaka N, Mihiro. T, Alexander H, Wolfgang. B. Controlling charge accumulation properties at organic heterointerfaces via spontaneous orientation polarization. Proc. IDW. 2023;30:580-583.

[5] Kondakov DY, Sandifer JR, Tang CW, Young RH. Nonradiative recombination centers and electrical aging of organic light-emitting diodes: direct connection between accumulation of trapped charge and luminance loss. J. Appl. Phys. 2003;93(2):1108-1119.